

Article

Electrical Defect State Distribution in Single Crystal ZnO Schottky Barrier Diodes

Jinhee Park ^{1,†}, You Seung Rim ^{2,†}, Pradeep Senanayake ³, Jiechen Wu ¹ and Dwight Streit ^{1,*}

¹ Department of Materials Science and Engineering, University of California, Los Angeles, CA 90095, USA; jinhee5park@ucla.edu (J.P.); jiechenwu1988@gmail.com (J.W.)

² School of Intelligent Mechatronics Engineering, Sejong University, Seoul 05006, Korea; youseung@sejong.ac.kr

³ Department of Electrical Engineering, University of California, Los Angeles, CA 90095, USA; pradeepnuwan@gmail.com

* Correspondence: streit@ucla.edu

† These authors equally contributed to this work.

Received: 19 December 2019; Accepted: 24 February 2020; Published: 27 February 2020



Abstract: The characterization of defect states in a hydrothermally grown single crystal of ZnO was performed using deep-level transient spectroscopy in the temperature range of 77–340 K. The native intrinsic defect energy level within the ZnO band gap occurred in the depletion region of ZnO Schottky barrier diodes. A major defect level was observed, with a thermal activation energy of 0.27 eV (E3) within the defect state distribution from 0.1 to 0.57 eV below the conduction band minimum. We confirmed the maximum defect concentration to be $3.66 \times 10^{16} \text{ cm}^{-3}$ at 0.27 eV (E3). As a result, we clearly confirmed the distribution of density of defect states in the ZnO band gap.

Keywords: Zinc oxide; Schottky Barrier Diode; DLTS; defect analysis

1. Introduction

Zinc oxide has attracted a lot of interest recently, due to its direct and wide band gap (3.4 eV at 300 K), high mobility, and simple processing, which make it suitable for optical applications such as light-emitting diodes (LEDs), and as a channel material for thin-film transistors (TFTs) in flat-panel displays [1–4]. While ZnO has a great deal of potential as a candidate for many optical applications, the electrical role of native defects in ZnO (e.g., Zn interstitial (Zn_i), Zn vacancy (V_{Zn}) and oxygen vacancy (V_O)) still remains unclear. It is also difficult to control the electrical defect properties and understand the exact mechanisms of carrier transport, which are associated with a complex defect distribution [5]. Native defects could extensively affect the electrical and optical properties of ZnO-based electronic devices. In particular, the role of defect distribution has been widely examined using photoluminescence (PL) [6], electron paramagnetic resonance (EPR) [7], admittance spectroscopy (AS) [8], and deep level transient spectroscopy (DLTS) [9–12].

Among these techniques, DLTS has a high sensitivity and is suitable for the analysis of defect states and impurities using Schottky diodes or p–n junction devices [13]. Therefore, the electronic defect states of ZnO have been intensively investigated using DLTS to find the evidence of intrinsic conductivity and the role of defect states. One of the most dominant defect states in n-type ZnO is the well-known V_O due to the relatively low formation energy of 3.5 eV. Recently, V_O has turned out to be a deep donor rather than a shallow donor [5]. Therefore, the origin of intrinsic n-type conductivity in undoped ZnO is believed not to be V_O . However, there is not a consensus regarding the source of the intrinsic n-type conductivity in undoped ZnO. Moreover, the explicit role of the defect states has not been fully explained, especially regarding the defect state distribution.

Up to now, very few papers have addressed the identity of defect states [9,14,15]. Additionally, none of these have confirmed the defect state distribution within the ZnO band gap. In this work, we have clearly confirmed the defect state distribution under the conduction band minimum (CBM) in the ZnO band gap. A summary of the prominent defect properties observed in ZnO using DLTS is shown in Table 1, compared with our result in the end row. In our method, we applied boiling H₂O₂ (prior to metal deposition) on the Zn-face (0001) of hydrothermally grown single-crystal ZnO, with Pd Schottky contacts to improve the Schottky contacts [8,16–19]. DLTS measurements were employed to investigate the defect state distribution. Defect energy levels with E3 (0.27–0.30 eV) and E4 (0.53 eV) in the ZnO Schottky barrier diodes (SBDs) have been confirmed in previous literature [20–23]. The major defect state of E3 (0.27 eV) below the CBM was also observed in our Pd/ZnO SBDs from the variations of the transient capacitance slope.

Table 1. Literature survey of the electronic properties of prominent defects investigated by deep level transient spectroscopy (DLTS) in as-grown ZnO; the defect energy level (E_t), defect concentration (N_t), capture cross section (σ_n) and oxygen vacancy (V_0).

Growth	E_c-E_t (eV)	N_t (cm ⁻³)	σ_n (cm ²)	Defect Identity (Year)
Hydrothermal [14]	0.278	2.1×10^{12}	0.3×10^{-14}	singly ionized V_0 , donor-like (1988)
Vapor-phase [13]	0.290	1.0×10^{14}	5.8×10^{-16}	maybe acceptor-like (2001)
Hydrothermal [9]	0.280	7.0×10^{14}	4.0×10^{-16}	maybe acceptor-like (2011)
Melt at high pressure [9]	0.280	3.5×10^{15}	4.0×10^{-16}	N/A (2011)
Hydrothermal	0.270	3.66×10^{16}	1.36×10^{-16}	This work

2. Experimental Methods

A hydrothermally grown single crystal of bulk ZnO with the (0001) Zn face up was used in this experiment. The Zn face has a lower amount of surface defect concentrations than the O face, which allows for a higher Schottky barrier height [18]. The carrier concentration, mobility, and resistivity of ZnO were measured at 0.86×10^{17} cm⁻³, 91.9 cm²·V⁻¹·s⁻¹, and 0.85 Ω·cm, respectively, through Hall effect measurements using the van der Pauw geometry (sample size of $10 \times 10 \times 5$ mm³).

The samples were cleaned in an ultrasonic bath with acetone, isopropyl alcohol (IPA), and de-ionized (DI) H₂O, sequentially. Before the metallization, the samples were placed into a boiling solution of 30% H₂O₂ for 3 min to improve the quality of the Schottky contacts, based on previous reports [8,19,23], and were blown using N₂ gas. As shown in Figure 1, annular ohmic contacts (inside diameter = 550 μm, outside diameter = 800 μm) and Schottky contacts (diameter 450 μm) were formed on the ZnO surface via electron-beam evaporation (base pressure of $\sim 10^{-6}$ mbar) and lift-off photolithography. Ti/Al/Pt/Au (20/80/40/80 nm) and Pd (60 nm) were deposited as ohmic and Schottky contacts, respectively [24]. The samples were then annealed at 200 °C for 1 min under an N₂ atmosphere. The Schottky contact area was 1.59×10^{-3} cm².

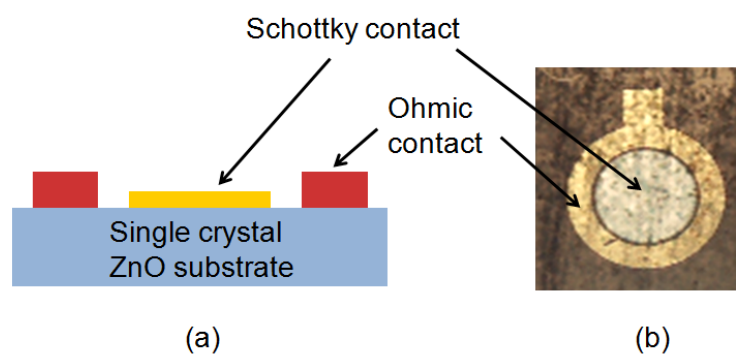


Figure 1. (Color Online) Simplified schematic illustration of the Pd/ZnO Schottky Barrier Diode (SBD): (a) Cross sectional view, (b) Top view (optical microscope image). Pd and Ti/Al/Pt/Au are used as Schottky and ohmic contacts, respectively.

Current–voltage (I–V), capacitance–voltage (C–V), and DLTS measurements were performed on the Pd/ZnO SBDs. The I–V and C–V measurements were carried out in the dark at room temperature using an Agilent 4156C Precision Semiconductor Parameter Analyzer, and an Agilent E4980A LCR meter. For the C–V measurement, the bias voltage was applied from 0 to –3 V, at 1 MHz. The measurement and data extraction of the DLTS (FT1030 DLTS, PhysTech GmbH, Moosburg, Germany) were followed in a previous report [13].

3. Results and Discussion

Figure 2 shows the I–V curve of the Pd/ZnO SBD. In order to form improved Schottky contacts on ZnO, a Schottky metal contact (e.g., Au, Ag, Pt, and Pd) on ZnO is required. However, the Schottky contact behavior of ZnO does not follow the work function difference directly due to unexpected surface defect states [5,16,17]. To overcome this problem, several techniques have been applied to the ZnO surface, such as oxygen plasma treatment, organic solvent cleaning and hydrogen peroxide (H₂O₂) treatment [8,18]. Among these treatments, the H₂O₂ treatment led to the surface defects of ZnO being significantly eliminated and the Schottky contacts between ZnO and metal being improved [8,19].

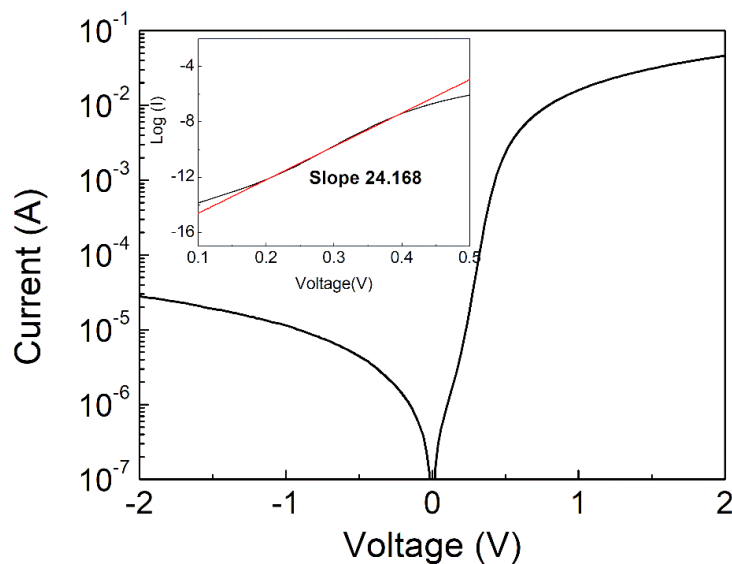


Figure 2. (Color Online) I–V characteristics of the Pd/ZnO SBDs from –3 to 2 V at room temperature. Ideality factor (n) is shown in the inset.

The leakage current was 2.8×10^{-5} A with a reverse bias of –2.5 V at room temperature. The leakage current was rectified over 10^3 , and reached 4.61×10^{-2} A at 2 V. Rectifying behavior was clearly shown in the Pd/ZnO SBDs. Typically, the calculation of the Schottky barrier height in diodes can be conducted using both I–V and C–V techniques, which are important to evaluate the diode performance. To calculate the Schottky barrier height in our devices, the saturation current (I_s) can be applied to the following equation [25]:

$$I_s = AA^* T^2 \exp\left(\frac{-\phi_B}{kT}\right) \quad (1)$$

where A , A^* , and ϕ_B represent the Schottky contact area (0.00159 cm^2), the effective Richardson constant, and the Schottky barrier height, respectively. The theoretical value of A^* in ZnO is $32 \text{ A}\cdot\text{cm}^{-2}\cdot\text{K}^{-2}$ based on an effective mass (m^*) of $0.27m_0$ [5]. The barrier height is calculated from I_s (1.6×10^{-7} A) at a zero bias from Equation (1). I_s was determined by extrapolating the curve of $\ln[I/(1-\exp(-qV/kT))]$ versus voltage under a forward bias up to $V = 0$ V. The calculated ϕ_B of our device was 0.85 eV, consistent with previous reports [18].

The ideality factor (n) is plotted by using the $\ln[I/(1-\exp(-qV/kT))]$ versus voltage curve as shown in the inset of Figure 2, and n is extracted from the slope of this curve for the evaluation of the

diode performance [25]. The current–voltage relationship for a Schottky diode can be expressed as $I = I_0[\exp(qV/nkT) - 1] \approx I_0 \exp(qV/nkT)$, and gives $\ln(I) = \ln(I_0) + qV/nkT$. Therefore, in this plot of $\ln(I)$ vs. V , the slope ($\partial V/\partial I$) can be extracted, and the ideality factor is calculated using the below equation. Here, we extracted the value of 1.49 in the linear region. This could be attributed to the carrier recombination, tunneling, or the interfacial layer between the metal and the semiconductor [5,26].

Figure 3 shows the C–V characteristics of the Pd/ZnO SBDs. We considered two factors, with built-in potential (V_{bi}) and carrier concentration (N_d) evaluated as follows: an approximate evaluation of V_{bi} was obtained using the intercept of the $1/C^2$ versus voltage plot, and N_d was also calculated from the slope of this plot (a). N_d was obtained using $2/(q\epsilon\epsilon_0 a)$, where q , ϵ , and ϵ_0 represent the elementary charge, the static dielectric constant (8.5 for ZnO), and the vacuum permittivity, respectively [25]. The calculated V_{bi} of the Pd/ZnO SBDs was 0.77 eV. Moreover, the carrier concentration of ZnO is $2.0 \times 10^{17} \text{ cm}^{-3}$, which is similar to the value obtained using Hall effect measurements ($0.86 \times 10^{17} \text{ cm}^{-3}$). The Schottky barrier height was in turn obtained using the following equation [25]:

$$\phi_B = q \left[V_{bi} + \frac{kT}{q} \ln \left(\frac{N_c}{N_d} \right) \right] \quad (2)$$

where N_c is the effective density of states of ZnO in the conduction band ($2.94 \times 10^{18} \text{ cm}^{-3}$ using $N_c = 2(2\pi m^* kT/h^2)^{3/2}$). The ϕ_B of our Pd/ZnO SBDs turned out to be 0.863 eV. The values of the Schottky barrier height showed very similar results, regardless of the measurement methods, which indicates that the Pd Schottky contact on ZnO was formed successfully. The detailed Schottky properties of the Pd/ZnO SBDs are listed in Table 2.

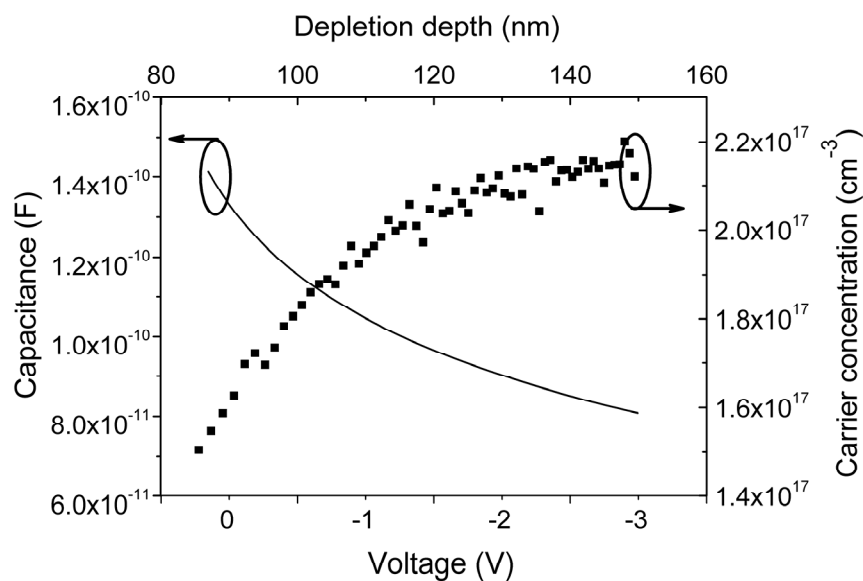


Figure 3. C–V characteristics of the Pd/ZnO SBDs as a function of reverse bias at 1 MHz. Carrier concentration versus depletion width is also plotted.

Table 2. The extracted parameters of the Pd/ZnO SBDs at room temperature: the ideality factor (n), reverse current (I_{rev}), barrier heights (ϕ_B), built-in voltage (V_{bi}) and carrier density (N_d).

Schottky Metal	n	I_{rev} at -1 V (A)	$\phi_{B, I-V}$ (eV)	$\phi_{B, C-V}$ (eV)	V_{bi} (V)	$N_{d, C-V}$ (cm^{-3})
Pd	1.49	1.14×10^{-5}	0.85	0.86	0.77	2.0×10^{17}

For the defect analysis of ZnO, we carried out DLTS measurements for the different temperature ranges from 77 to 340 K at a frequency of 1 MHz. Applied reverse bias voltage was used at -2.5 V to form of a strong depletion region and forward bias voltage was then applied at 0 V with a filling pulse

time width (t_p) of 50 ms, as shown in Figure 4a. The transient capacitance was measured to within 40 ms at different temperatures from 77 to 340 K (corresponding to 0.1–0.57 eV below the conduction band (E_c)). The maximum transient capacitances were extracted by using different emission rates (e_n) (emission rate = $\ln(t_1/t_2)/(t_2-t_1)$, where t_1 and t_2 are the start and end of the time window), and emission rates of 0.034, 0.042, 0.093, 0.423, and 0.888 ms^{-1} were selected as shown in Figure 4b. In addition, emission rates (e_n) can also be determined using the equation below [25]:

$$e_n/T^2 = \gamma_n \sigma_n \times \exp(-((E_c - E_t)/KT))$$

with $\gamma_n = (v_{th}/T^{1/2})(N_c/T^{3/2}) = 3.25 \times 10^{21} (m_n/m_0) \text{ cm}^{-2} \cdot \text{s}^{-1} \cdot \text{K}^{-2}$, where m_n is the electron density of-states effective mass and m_0 is the electron rest mass. At different settings of t_1 and t_2 , the DLTS signal gave out a different set of emission rates for the different temperatures. By using an Arrhenius plot of $\ln(e_n/T^2)$ vs. $1/T$, the trap energy level (E_t) and capture cross-section (σ_n) were obtained. The Arrhenius plot had a slope of $-(E_c - E_t)/K$, determining E_t , and an intercept on the $\ln(e_n/T^2)$ axis of $\ln(\gamma_n \sigma_n)$, determining σ_n . We calculated the defect energy level (E_t) and capture cross section (σ_n) by using the Arrhenius plot as shown in Figure 4c. Therefore, we confirmed that the E_t and σ_n of ZnO were $E_c - 0.27$ eV (labeled E3) and $1.36 \times 10^{-16} \text{ cm}^2$, respectively [9,20]. It is well known that ZnO has various defect energy levels originating from non-stoichiometry (e.g., Zn_i , V_{Zn} , Oxygen antisite (O_{Zn} or V_0), etc.) [27–30].

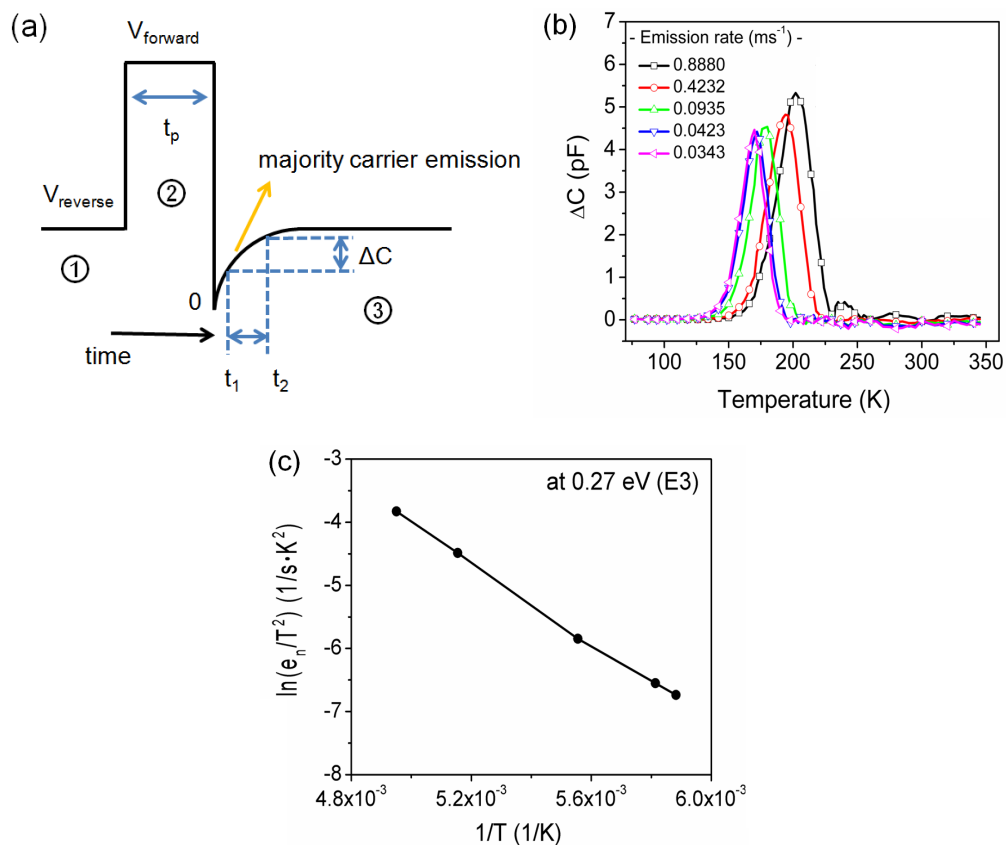


Figure 4. (Color online) (a) Applied voltage and resultant transient capacitance; (b) DLTS spectra of the Pd/ZnO SBDs samples under different emission rates from 0.0343 ms^{-1} ($t_1 = 20.2$ ms, $t_2 = 40.4$ ms) to 0.8880 ms^{-1} ($t_1 = 0.78$ ms, $t_2 = 1.56$ ms); (c) Arrhenius plot of the level E3.

This transient capacitance behavior may have been caused by the positively charged defects through the thermal emission of carriers in the depletion region, and by decreased depletion width due to the increase in total charge density, as shown in Figure 5a–c. This is because the donor-type

defect is positively ionized when it is unoccupied and neutral when it is filled with an electron [25]. In this manner, the signal gives out a different set of emission rates and temperatures. The trap emits carriers at this emission rate. As a result, transient capacitance was increased. This phenomenon is in agreement with those obtained from previous reports [27,31]. However, the origin of these defects is still unclear and complex. It requires further study to find the precise evidence of the defect formation.

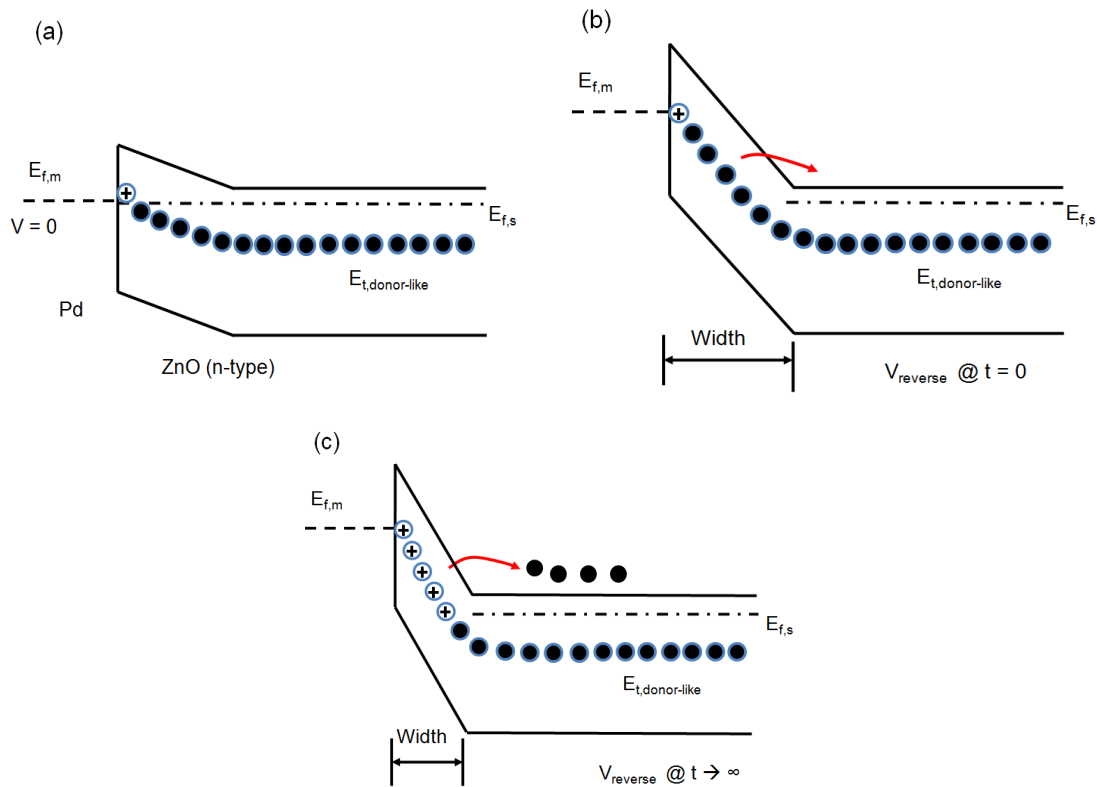


Figure 5. (Color online) A Schottky diode for majority carrier emission; (a) zero bias (forward bias), (b) reverse bias at $t = 0$, (c) reverse bias as $t \rightarrow \infty$.

Typically, both interface and bulk-trap states can contribute to the DLTS signal in a Schottky junction. Although it was difficult to extract only the bulk traps, due to the overlapping of the electron emissions from the interface states ($\sim 10^{14} \text{ cm}^{-2}$), the interface state density was much weaker than that of the bulk defect states ($\sim 10^{17} \text{ cm}^{-3}$) [32]. Therefore, the predominant defect formation could be defined within the bulk ZnO. Based on DLTS of the Pd/ZnO SBDs, we clearly observed the change of the transient capacitance from 77 to 340 K and predicted the defect states' distribution between 0.1 and 0.57 eV below the CBM.

The DLTS signal reflects the distribution of the signal originated from each defect energy level. Hence, the DLTS signal is simply proportional to the defect concentration (N_t) given by the equation [13,25]:

$$N_t = 2N_d \frac{\Delta C_{\max}}{C_0} \quad (3)$$

where N_d , ΔC_{\max} , and C_0 represent the carrier concentration, maximum transient capacitance amplitude, and capacitance of the device at -2.5 V ($C_0 = 85 \text{ pF}$), respectively. The temperature range from 77 to 340 K can also be related to the defect energy level from 0.1 to 0.57 eV below the CBM, and the defect distribution can be calculated by the electron emission rate equation [13,25,30,33]:

$$E_c - E_t = kT \ln(\sigma_n \nu_{\text{th}} N_c \tau_0) \quad (4)$$

where kT , σ_n , v_{th} , and τ_0 represent the thermal energy, electron capture cross-section area of the trap (assumed to be 10^{-16} cm²), electron thermal velocity, and emission time constant approximated to be half of the time width used in the measurements ($\tau_0 = 20$ ms), respectively [33]. Calculated defect concentration and distribution are shown in Figure 6. Scattering and noise within the data seemed to be due to thermal instability. We confirmed the maximum defect concentration to be 3.66×10^{16} cm⁻³ at 0.27 eV from the CBM.

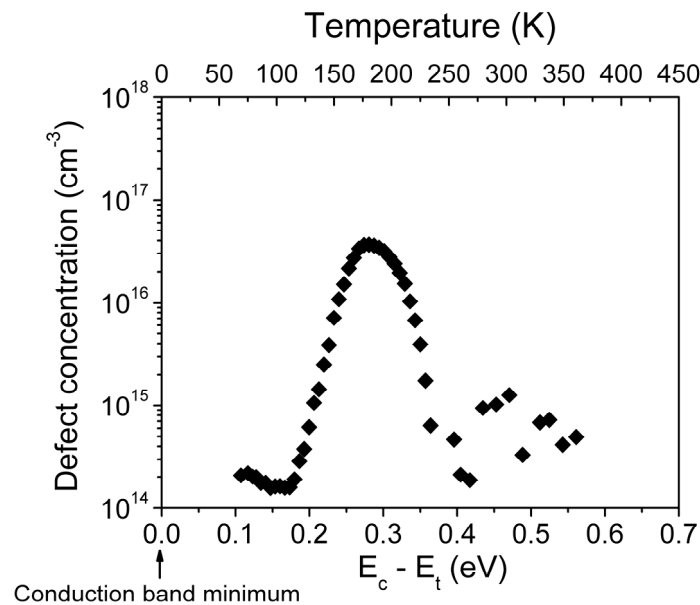


Figure 6. (Color online) The correspondent subgap density of states as a function of defect energy from the conduction band.

4. Conclusions

We investigated single-crystal ZnO SBDs and carried out a DLTS analysis to find the defect state distribution in the ZnO band gap. We confirmed that a Schottky barrier height of 0.85 eV with a Pd contact was formed on the Pd/ZnO SBDs. Compared to previous reports, our ZnO SBDs have a similar defect energy level of $E_c - 0.27$ eV below the CBM. Although the origin of defects is still unclear and more studies are needed, we believe that complex oxygen-related defects could possibly be the source of defects near the conduction band of single crystal ZnO (in the Pd/ZnO SBDs). Finally, we successfully obtained a defect state distribution below the conduction band in the range of 0.1–0.57 eV. The maximum defect concentration was 3.66×10^{16} cm⁻³, 0.27 eV from the CBM.

Author Contributions: Conceptualization, writing, and experiments J.P. and Y.S.R.; methodology and analysis, P.S., J.W.; supervision and editing, D.S. All authors have read and agreed to the published version of the manuscript.

Funding: Financial support was provided by the University of California, Los Angeles (UCLA) school of engineering, Samsung, and Basic Science Research Program through the National Research Foundation of Korea (NRF), funded by the Ministry of Education (2017R1D1A1B03030818).

Acknowledgments: J.H. Park and Y.S. Rim equally contributed to this work. Financial support was provided by the University of California, Los Angeles (UCLA) school of engineering and Samsung. We would also like to thank the Nanoelectronics Research Facility (NRF), acknowledge the use of the Integrated Systems Nanofabrication Cleanroom (ISNC) at the California NanoSystems Institute (CNSI) in UCLA, and thank the Basic Science Research Program through the National Research Foundation of Korea (NRF), funded by the Ministry of Education (2017R1D1A1B03030818), for making the fabrication of this device possible. Special thanks to Alan Farrell and Diana Huffaker for their support.

Conflicts of Interest: The authors declare no conflict of interest.

References

- Jagadish, C.; Pearton, S.J. *Zinc Oxide Bulk, Thin Films and Nanostructures: Processing, Properties, and Applications*, 1st ed.; Elsevier: Oxford, UK, 2006.
- Wager, J.F. Transparent electronics. *Science* **2003**, *300*, 1245–1246. [[CrossRef](#)]
- Fortunato, E.; Barquinha, P.; Pimentel, A.; Goncalves, A.; Marques, A.; Pereira, L.; Martins, R. ACMBG Pimentel, AMF Goncalves, AJS Marques and LMN Pereira. *Adv. Mater.* **2005**, *17*, 590. [[CrossRef](#)]
- Monakhov, E.V.; Kuznetsov, A.Y.; Svensson, B.G. Zinc oxide: Bulk growth, role of hydrogen and Schottky diodes. *J. Phys. D: Appl. Phys.* **2009**, *42*, 153001. [[CrossRef](#)]
- Özgür, Ü.; Alivov, Y.I.; Liu, C.; Teke, A.; Reshchikov, M.A.; Doğan, S.; Avrutin, V.; Cho, S.J.; Morkoç, H. A comprehensive review of ZnO materials and devices. *J. Appl. Phys.* **2005**, *98*, 041301. [[CrossRef](#)]
- Zeuner, A.; Alves, H.; Hofmann, D.M.; Meyer, B.K.; Heuken, M.; Bläsing, J.; Krost, A. Structural and optical properties of epitaxial and bulk ZnO. *Appl. Phys. Lett.* **2002**, *80*, 2078. [[CrossRef](#)]
- Hofmann, D.M.; Hofstaetter, A.; Leiter, F.; Zhou, H.; Henecker, F.; Meyer, B.K.; Orlinskii, S.B.; Schmidt, J.; Baranov, P.G. Hydrogen: A relevant shallow donor in zinc oxide. *Phys. Rev. Lett.* **2002**, *88*, 045504. [[CrossRef](#)]
- Schifano, R.; Monakhov, E.V.; Grossner, U.; Svensson, B.G. Electrical characteristics of palladium Schottky contacts to hydrogen peroxide treated hydrothermally grown ZnO. *Appl. Phys. Lett.* **2007**, *91*, 193507. [[CrossRef](#)]
- Scheffler, L.; Kolkovskiy, V.I.; Lavrov, E.V.; Weber, J. Deep level transient spectroscopy studies of n-type ZnO single crystals grown by different techniques. *J. Phys.: Condens. Matter* **2011**, *23*, 334208. [[CrossRef](#)]
- Chicot, G.; Muret, P.; Santailier, J.-L.; Feuillet, G.; Pernot, J. Oxygen vacancy and EC– 1 eV electron trap in ZnO. *J. Phys. D: Appl. Phys.* **2014**, *47*, 465103. [[CrossRef](#)]
- Gür, E.; Coşkun, C.; Tüzemen, S. High energy electron irradiation effects on electrical properties of Au/n-ZnO Schottky diodes. *J. Phys. D: Appl. Phys.* **2008**, *41*, 105301. [[CrossRef](#)]
- Ohbuchi, Y.; Kawahara, T.; Okamoto, Y. Morimoto, Distributions of Interface States and Bulk Traps in ZnO Varistors. *J. Jpn. J. Appl. Phys.* **2011**, *40*, 213. [[CrossRef](#)]
- Lang, D.V. Fast capacitance transient apparatus: Application to ZnO and O centers in GaP p-n junctions. *J. Appl. Phys.* **1974**, *45*, 3023. [[CrossRef](#)]
- Auret, F.D.; Goodman, S.A.; Hayes, M.; Legodi, M.J.; Laarhoven, H.A.V.; Look, D.C. The influence of high energy proton bombardment on the electrical and defect properties of single-crystal ZnO. *J. Phys.: Condens. Matter* **2001**, *13*, 8989.
- Rucavado, E.; Jeangr, Q.; Urban, D.F.; Holovský, J.; Remes, Z.; Duchamp, M.; Landucci, F.; Dunin-Borkowski, R.E.; Körner, W.; Elsässer, C.; et al. Enhancing the optoelectronic properties of amorphous zinc tin oxide by subgap defect passivation: A theoretical and experimental demonstration. *Phys. Rev. B* **2017**, *95*, 245204. [[CrossRef](#)]
- Sheng, H.; Muthukumar, S.; Emanetoglu, N.W.; Lu, Y. Schottky diode with Ag on (1120) epitaxial ZnO film. *Appl. Phys. Lett.* **2002**, *80*, 2132. [[CrossRef](#)]
- Allen, M.W.; Alkai, M.M.; Durbin, S.M. Metal Schottky diodes on Zn-polar and O-polar bulk ZnO. *Appl. Phys. Lett.* **2006**, *89*, 103520. [[CrossRef](#)]
- Brillson, L.J.; Lu, Y. ZnO Schottky barriers and Ohmic contacts. *J. Appl. Phys.* **2011**, *109*, 121301. [[CrossRef](#)]
- Schifano, R.; Monakhov, E.V.; Svensson, B.G.; Diplas, S. Surface passivation and interface reactions induced by hydrogen peroxide treatment of n-type ZnO (000 1). *Appl. Phys. Lett.* **2009**, *94*, 132101. [[CrossRef](#)]
- Fang, Z.-Q.; Clafin, B.; Look, D.C.; Dong, Y.F.; Mosbacher, H.L.; Brillson, L.J. Surface traps in vapor-phase-grown bulk ZnO studied by deep level transient spectroscopy. *J. Appl. Phys.* **2008**, *104*, 063707. [[CrossRef](#)]
- Auret, F.D.; Nel, J.M.; Hayes, M.; Wu, L.; Wesch, W.; Wendler, E. Electrical characterization of growth-induced defects in bulk-grown ZnO. *Superlatt. Microstruct.* **2006**, *39*, 17. [[CrossRef](#)]
- Vines, L.; Monakhov, E.V.; Svensson, B.G. Effect of high temperature treatments on defect centers and impurities in hydrothermally grown ZnO. *Physica B* **2009**, *404*, 4386. [[CrossRef](#)]
- Gu, Q.L.; Ling, C.C.; Chen, X.D.; Cheng, C.K.; Ng, A.; Beling, C.D.; Fung, S.; Djurišić, A.B.; Lu, L.W.; Brauer, G.; et al. Hydrogen peroxide treatment induced rectifying behavior of Au/n-ZnO contact. *Appl. Phys. Lett.* **2007**, *90*, 122101. [[CrossRef](#)]

24. Ip, K.; Thaler, G.T.; Yang, S.; Han, H.S.; Li, Y.; Norton, D.P.; Pearton, S.J.; Jang, S.F.; Ren, J. Contacts to ZnO. *Cryst. Growth* **2006**, *287*, 149. [[CrossRef](#)]
25. Schroder, D.K. *Semiconductor Material and Device Characterization*, 3rd ed.; John Wiley & Sons, Inc.: Hoboken, NJ, USA, 2006.
26. Sze, S.M.; Ng, K.K. *Physics of Semiconductor Devices.*, 3rd ed.; John Wiley & Sons, Inc.: Hoboken, NJ, USA, 2007.
27. Janotti, A. and Van de Walle, C.G. Native point defects in ZnO. *Phys. Rev. B* **2007**, *76*, 165202. [[CrossRef](#)]
28. Kohan, A.F.; Ceder, G.; Morgan, D.; Van de Walle, C.G. First-principles study of native point defects in ZnO. *Phys. Rev. B* **2000**, *61*, 15019. [[CrossRef](#)]
29. Janotti, A.; Van de Walle, C.G. Oxygen vacancies in ZnO. *Appl. Phys. Lett.* **2005**, *87*, 122102. [[CrossRef](#)]
30. Janotti, A.; Van de Walle, C.G. Fundamentals of zinc oxide as a semiconductor. *Rep. Prog. Phys.* **2009**, *72*, 126501. [[CrossRef](#)]
31. Look, D.C.; Hemsley, J.W.; Sizelove, J.R. Residual native shallow donor in ZnO. *Phys. Rev. Lett.* **1999**, *82*, 2552. [[CrossRef](#)]
32. Brillson, L.J. *Semiconductors and Semimetals: Oxide Semiconductors*, 1st ed.; Svensson, B.G., Pearton, S.J., Eds.; SEMSEM; Academic Press: San Diego, CA, USA, 2013.
33. Chasin, A.; Simoen, E.; Bhoolokam, A.; Nag, M.; Genoe, J.; Gielen, G.; Heremans, P. Deep-level transient spectroscopy on an amorphous InGaZnO₄ Schottky diode. *Appl. Phys. Lett.* **2014**, *104*, 082112. [[CrossRef](#)]



© 2020 by the authors. Licensee MDPI, Basel, Switzerland. This article is an open access article distributed under the terms and conditions of the Creative Commons Attribution (CC BY) license (<http://creativecommons.org/licenses/by/4.0/>).